Strain hardening, avalanches, and strain softening in dense cross-linked actin networks

Jan A. Åström,[1] P. B. Sunil Kumar,[2,3] Ilpo Vattulainen,[3,4,5] and Mikko Karttunen[6]
[1]*CSC—Finnish IT Center for Science, Esbo, Finland*
[2]*Department of Physics, Indian Institute of Technology Madras, Chennai 600036, India*
[3]*Memphys—Center for Biomembrane Physics, Physics Department, University of Southern Denmark, Odense, Denmark*
[4]*Department of Physics and Helsinki Institute of Physics, Helsinki University of Technology, Helsinki, Finland*
[5]*Department of Physics, Tampere University of Technology, Tampere, Finland*
[6]*Department of Applied Mathematics, The University of Western Ontario, London, Ontario, Canada*
(Received 30 March 2007; revised manuscript received 25 January 2008; published 16 May 2008)

Actin filament networks enable the cytoskeleton to adjust to internal and external forcing. These dynamic networks can adapt to changes by dynamically adjusting their cross-links. Here, we model actin filaments as cross-linked elastic fibers of finite dimensions, with the cross-links being approximately 1 μm apart, and employ a full three-dimensional model to study their elastic properties by computer simulations. The results show compelling evidence that dense actin networks are characterized by (a) strain hardening without entropic elasticity, (b) avalanches of cross-link slippage leading to strain softening in the case of breakable cross-links, and (c) spontaneous formation of stress fibers in the case of dynamic cross-link formation and destruction.

DOI: 10.1103/PhysRevE.77.051913 PACS number(s): 87.16.Ka, 87.16.A−, 91.60.Ba

I. INTRODUCTION

Biological cells have an amazing capacity to change their shape and to adjust to a variety of external conditions. The dynamical structural organization associated with these processes is believed to be facilitated by a meshlike structure formed of protein filaments, active and passive cross-linkers, and a chemical network that is able to control the amount of cross-linking and filament lengths [1]. In cells, that dynamical structure is the cytoskeleton. The fact that cellular response is controlled by a meshlike structure with a dynamic cross-link density makes it extraordinarily different from conventional human-engineered elastic networks.

Actin filaments constitute one of the major components of the cytoskeleton. From a mechanistic point of view, actin networks stiffen and rigidify cells, thus helping them to resist deformations. These networks exhibit complex physical properties such as viscoelasticity [2–5], and they also render a variety of biological functions possible, including the action of motor proteins and self-organization [6]. Cellular motion is largely related to the mechanical properties of the cytoskeleton [1,7–9], cell division involves changes in the network cross-links, and cytoskeletal actin networks transmit intra- and intercellular signals by their (visco)elastic response [5,10].

The above aspects have motivated a number of recent experimental and theoretical studies on semiflexible polymers and their networks [3,4,10–17]. Another class of models based on prestressed filaments has also been proposed [18]. Perhaps surprisingly, quantitative understanding of the elastic properties of actin networks is still in its infancy. Significant deviations from predictions of single-filament-based models [11], which have been successful in modeling systems with low levels of cross-linking, have been observed in experiments with moderately and highly cross-linked actin networks [3,4]. This and the fact that nonlinear response of cross-linked semiflexible filaments is nonuniversal and can be tuned by many parameters [3], necessitates a need for modeling actin filament networks from different points of view.

Nonlinearity and nonaffinity are incorporated into models for two-dimensional cross-linked semiflexible polymer networks by using serial connection of springs between cross-linking points to incorporate two stretching modes and a bending mode, with three different moduli [19]. Here we follow a different approach and use a full three-dimensional model of cross-linked elastic beams to address two problems inherent in actin networks: (1) their *connectivity* and their *dense nature*, and (2) the *dynamic nature* of cytoskeleton networks. In nature, the cross-linker itself is dynamic, with a characteristic on-off time scale. This feature is not included in the model described here. However, the density of cross-links may change due to extra- and intracellular changes affecting the connectivity and rheological properties [2,5] of the network. We allow for this dynamical change of network topology by incorporating a maximum and minimum value of the cross-linker length, for breaking and making the cross-links, respectively. Recently, Gardel *et al.* [16] showed how changes in the density of cross-links and actin concentration affect the elastic modulus of the system. Interestingly, they also discussed the possibility of a new elastic regime where no general mechanism for strain hardening can be identified—they suggested that in that regime the properties of the filaments control the behavior. As will be discussed later, our findings render some support to this idea and they provide a physical mechanism to rationalize strain hardening for dense networks. Since the typical mesh size of the cytoskeletal network is about 100 nm [20], it is reasonable to consider segments of actin, having a typical persistence length of about 15 μm, as stiff elastic rods [21].

As for the dynamical nature of these networks, microrheology experiments indicate strong changes in the local structure of the cytoskeleton upon application of oscillatory shear [22]. These structural changes may be due to the action of motors as well as passive cross-linkers. Since changes in geometry in response to an externally imposed strain are an important feature of the cytoskeleton, it is crucial to account

for these aspects. For example, it has been pointed out that nonaffine network rearrangements can lead to strain stiffening in two-dimensional cross-linked actin networks [23]. It has also been pointed out that action of motors can change the tension on the fibers and hence contribute to an overall increase in stiffness of the network. Such an increase in stiffness has been observed in actin networks, permanently cross-linked by biotin and neutravidin, in the presence of the molecular motors myosin and ATP [24].

II. MODELS AND METHODS

Here, we introduce a full three-dimensional (3D) computational model which allows a systematic increase in complexity to address the physical mechanisms behind the above issues. Changes in geometry and the dynamic nature of the networks are taken into account. The model consists of stiff fibers randomly located and oriented in 3D with springs as cross-links at locations where two fibers intersect. In our model, we increase complexity in the following sequence. (1) First we include only passive cross-links which are formed at zero imposed strain and cannot break or move. This is essentially similar to the model introduced by Onck *et al.* [23], but now with beams of finite size. (2) We then make the cross-links, which are first formed at zero imposed strain, "semipassive," by allowing them to break when strained beyond the maximum length. (3) In the next level of complexity, the dynamic cross-links are able to break, when strained beyond a limit, and form, if two fibers come close enough to each other during straining (notice that these cross-links do not have a rate for spontaneous detachment, i.e., detachment is purely strain driven). We will now describe these models in some detail.

The model is based on a full description of a 3D elastic network, and describes the cytoskeleton in terms of randomly placed filaments linked together at their crossing points. All filaments are considered to be identical and straight under zero loading conditions. Individual filaments have a finite length and width. The fiber density ρ is defined as the average number of filaments in a volume of size L^3, where L is the length of an individual filament. Boundary conditions were chosen such that the y and z directions are free, while the ends of the mesh are clamped in the x direction. Strain is applied in the x direction. The mass of each fiber is discretized by a set of points (of mass m) at equal distances along the fiber. Each pair of mass points, belonging to different fibers and closer than some threshold (δl), are linked with a spring. That is how cross-links are defined. The mesh obtained through this deposition process is taken as the intial configuration.

A segment, bounded by two mass points, can be deformed either by different translational motion of the end points of the segment or by rotation of the end points. In constructing the stiffness matrix $\mathbf{K}$ we use the Euler-Bernoulli beam theory, which takes into account stretching, bending, transverse deformation, and torsional deformation of the segments [25]. The aspect ratios of all actin segments are larger that 30, in which case shear deformation can be neglected. The stiffness matrix ($\mathbf{K}$) of a single segment is of size 12 $\times 12$, where the columns correspond to the three translational and three rotational degrees of freedom for the two end points of the segment [26]. The stiffness matrix for a segment in a different orientation is constructed by a similarity transformation. To construct the full stiffness matrix for the mesh, the individual $\mathbf{K}$'s are expanded (with zeros) to include all the degrees of freedom of the entire mesh and added together. The $\mathbf{K}$ matrix is given as

$$\begin{bmatrix}
\alpha & 0 & 0 & 0 & 0 & 0 & -\alpha & 0 & 0 & 0 & 0 & 0 \\
0 & \beta & 0 & 0 & 0 & \gamma & 0 & -\beta & 0 & 0 & 0 & \gamma \\
0 & 0 & \beta & 0 & -\gamma & 0 & 0 & 0 & -\beta & 0 & -\gamma & 0 \\
0 & 0 & 0 & \zeta & 0 & 0 & 0 & 0 & 0 & -\zeta & 0 & 0 \\
0 & 0 & -\gamma & 0 & \eta & 0 & 0 & 0 & \gamma & 0 & \omega & 0 \\
0 & \gamma & 0 & 0 & 0 & \eta & 0 & -\gamma & 0 & 0 & 0 & \omega \\
-\alpha & 0 & 0 & 0 & 0 & 0 & \alpha & 0 & 0 & 0 & 0 & 0 \\
0 & -\beta & 0 & 0 & 0 & -\gamma & 0 & \beta & 0 & 0 & 0 & -\gamma \\
0 & 0 & -\beta & 0 & \gamma & 0 & 0 & 0 & \beta & 0 & \gamma & 0 \\
0 & 0 & 0 & -\zeta & 0 & 0 & 0 & 0 & 0 & \zeta & 0 & 0 \\
0 & 0 & -\gamma & 0 & \omega & 0 & 0 & 0 & \gamma & 0 & \eta & 0 \\
0 & \gamma & 0 & 0 & 0 & \omega & 0 & -\gamma & 0 & 0 & 0 & \eta
\end{bmatrix},$$

where $\alpha=\frac{EA}{L_s}$, $\beta=\frac{12EI}{L_s^3}$, $\gamma=\frac{6EI}{L_s^2}$, $\zeta=\frac{GI_r}{L_s}$, $\eta=\frac{4EI}{L_s}$, $\omega=\frac{2EI}{L_s}$, E is Young's modulus, A is the cross-sectional area, and L_s is the length of the filament segment. I is the moment of inertia with respect to a cross-sectional symmetry axis (assumed to be similar in at least two directions). I_r is the moment of inertia with respect to the center point of the cross section. It is given by $I_r=\int_0^r dA' r'^2$, where r is the radius of the beam and dA' is the differential cross-sectional area of an element. The torsion modulus is given by GI_r/L, where $G=E/2(1+\nu)$ is the shear modulus with ν being the Poisson ratio. All lengths are measured in units of L, the length of a filament thus being $L=1$. The thickness of the filament was chosen to be $w=0.003$, mass $m=1\times10^{-4}$, damping $c=1\times10^{-4}$, and Young's modulus $E=6\times10^3$. These parameters also set the time scale of the simulations.

Global strain is applied by moving the opposite boundaries in the x direction by $\pm\delta x$, where δx is a function of time t. The equation of motion for the deformation field of the mesh is a discrete version of Newton's equation of motion with dissipation,

$$\mathbf{M}\ddot{\vec{r}} + \mathbf{C}\dot{\vec{r}} + \mathbf{K}\vec{r} = \vec{0}. \tag{1}$$

Here, the term for viscous damping, $\mathbf{C}$, is a diagonal matrix containing the damping coefficients, and $\mathbf{M}$ describes the inertia of the links. The column vector $\vec{r}$ contains the position vectors of all mass points. Since the time derivaties of $\vec{r}$ remain small at all times, we use the diagonal (or so-called lumped mass and damping matrices) instead of the consistent mass and damping matrices with off-diagonal elements; see, e.g., Refs. [27,28]. A fairly similar approach has been used by Ziebert and Aranson [29].

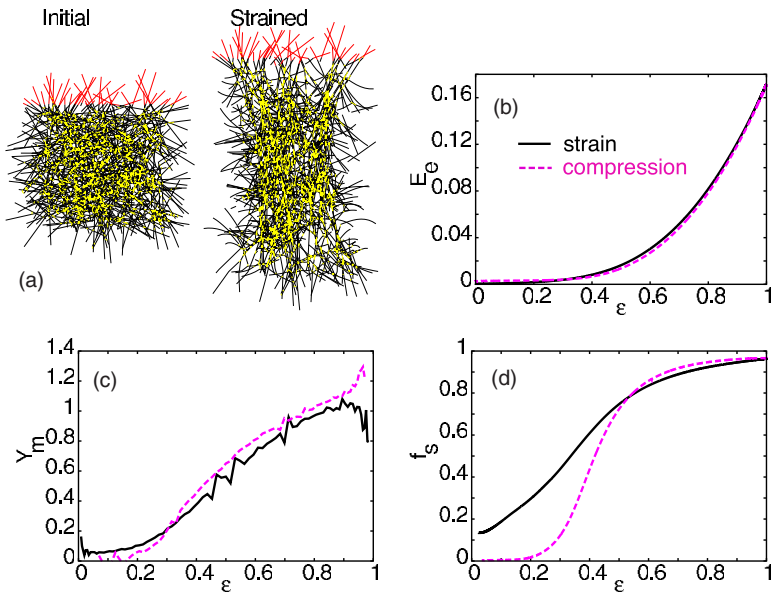

FIG. 1. (Color online) (a) Snapshots of a mesh with passive cross-links at zero (left) and 100% strain (right). (b) Elastic energy (E_e) of the fibers for the mesh in (a) as a function of strain ϵ. (c) Second numerical derivative of the curve in (b) with respect to ϵ (Young's modulus of the mesh, Y_m) as function of strain ϵ. (d) Fraction of elastic energy of the fibers related to fiber stretching (as opposed to torsion, bending, etc.) (f_s) as a function of strain ϵ. f_s is approximately 0.15 at $t=0.0$ and vanishes after a full strain cycle.

As the mass points move in discrete time steps according to Eq. (1), the segments deform and the network geometry changes. It is quite obvious that in a fiber-mesh material, constructed of slender fibers with a lot of empty space in between, the fibers with originally random orientation will begin to align themselves in the stretching direction as strain increses. This implies that the stiffness matrix evolves in time. Changes in the stiffness matrix imply that **K** is also a function of $\vec{r}$ and hence the equation of motion becomes nonlinear through the third term in Eq. (1), which becomes $\int_0^t \mathbf{K}(\vec{r}(t))\vec{r}(t)dt$.

While the rotation and translation of the individual actin segments can be large, the elastic deformations remain small. Therefore, and for simplicity, we do not include nonlinear higher-order terms in the calculation of the elastic deformation forces. The "geometrical stiffness," which refers to nonlinear elasticity of beams related to, e.g., buckling, is accounted for by dividing each actin fiber into 10–20 segments, each modeled by an Euler-Bernoulli beam.

To model cross-links that can break, we chose $\delta l=0.06$ as the threshold value for the linking distance. The members of each pair of mass points belonging to different filaments which are closer than δl are linked with a spring of stiffness $K_l=2\times10^{-1}$. The equilibrium lengths of these springs were set to $\delta l_0=0.04$, implying that cross-links must be stretched by 50% to reach the breaking threshold of $\delta l=0.06$. In the case of fully dynamic cross-links, as the mesh deforms, new pairs of mass points come within δl and new links are formed.

III. RESULTS

A. Passive cross-links

We first consider the simplest case, namely, the model with passive cross-links only. Snapshots of the original unstrained mesh and the mesh strained 100% are shown in Fig. 1(a) together with the elastic energy as function of strain $[E_e(\epsilon)]$ in Fig. 1(b). Figure 1(b) reveals that mesh deformation is almost reversible. There is only a small hysteresis as a result of the viscotic damping of the mesh [see Eq. (1)]. The second derivative of the elastic energy curve with respect to strain gives the stiffness of the mesh as function of strain, $Y_m(\epsilon)$, and is shown in Fig. 1(c). This figure reveals significant strain hardening of the mesh, similar to that seen by Onck *et al.* [23].

To resolve the origin of the strain dependence of stiffness, we determined the fraction f_s of the total elastic energy associated with stretching of the filaments (as opposed to other types of deformation like transverse deformation or bending); that is, the fraction of the total deformation energy of the fibers associated with the change in length of the segments [13,15,30,31]. This ratio, known as the affine measure, is shown as function of strain in Fig. 1(d). At small times, i.e., at small strain, the energy is due to the initial pulling of the links. At this stage f_s is about 15%. As strain increases to 100%, f_s increases to over 95%. When the mesh is compressed back toward zero strain, f_s vanishes. The stiffness for elongation of the fibers is given as Ew^2/l, while the transverse deformation stiffness is Ew^4/l^3. For slender fibers (i.e., $w/l \ll 1$) this means that an increase in f_s will result in strain hardening, as can be seen from Fig. 1(c).

B. Semipassive cross-links: Rupture avalanches

Let us now use the same mesh as above and change the cross-links to semipassive ones, i.e., they can break. Figure 2(a) shows snapshots of the system. As expected, for small strains, the elastic energy as a function of strain is identical to the previous case of passive cross-links [Fig. 1(b)]. Once strain is increased and the links begin to break, the energy drops as is seen in Fig. 2(b). Figure 2(a) shows that the mesh ruptures close to the clamped boundaries. This indicates that clamping causes a slight increase of stresses close to the boundary.

Rupture of the individual links is strongly correlated. The strain distribution ($\delta\epsilon$) between ruptures is roughly a power law with an exponential cutoff in the distribution for large $\delta\epsilon$

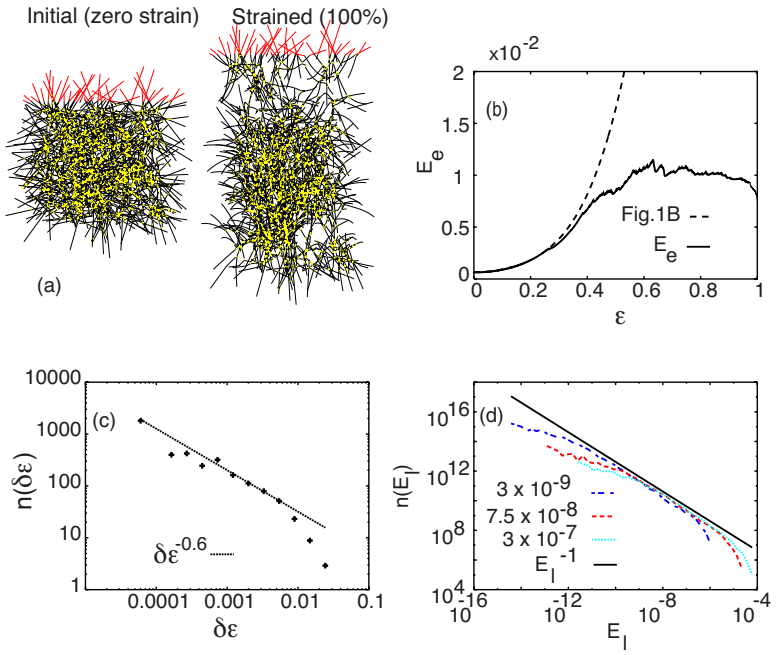

FIG. 2. (Color online) (a) Snapshots of a mesh with semipassive cross-links at zero strain (left) and 100% strain. (b) Elastic energy (E_e) of the fibers in mesh in (a) as a function of strain. Dotted line: curve from Fig. 1(b) for comparison. (c) Length distribution of the strain increase intervals between adjacent link fractures for semipassive links $n(\delta\epsilon)$. (d) Elastic energy distribution of the links for small strain (i.e., before any link fractures), $n(E_l)$. The distribution functions are approximately power laws with $n(E_l) \propto E_l^{-1}$ with cutoffs at small and large strains. Three distributions are displayed: $\epsilon = 3 \times 10^{-9}$, 7.5×10^{-8}, 3×10^{-7}. As ϵ increases, the cutoffs move to larger energies.

[Fig. 2(c)]. Qualitatively, this is similar to ruptures in models for earthquakes and paper and slow fracture in brittle materials [32–36].

Next, we study the distribution of elastic energy stored in the cross-links. For small strains, i.e., before any rupture events occur, the energy distribution is very broad. The distribution function is a power law with an exponent close to unity [Fig. 2(d)] over several orders of magnitude. Such a distribution is maximally broad as it is marginally normalizable. That means that there is no well-defined average energy for a contact but the energy is very broadly distributed [37]. A cross-link fracture may trigger fractures of other cross-links, thus causing small avalanches. All fractures are irreversible for semipassive cross-links with the stiffness vanishing when the mesh is completely broken.

C. Dynamic cross-links

Finally, we look at the case of fully dynamic cross-links. The starting mesh, at time $t=0$, is the same as used in the case of passive and semi-passive cases, but the links can now break and reform. At time $t=0$, only a fraction of the links are connected. When the mesh is strained, the fibers align in the direction of the strain and move close to each other. This leads to an increase in the number of cross-links as new ones can form when two segments come closer than δl to each other. For dynamic links, this causes the fibers to spontaneously form bunches in the direction of straining, similar to the mechanical-stretch-induced stress fiber organization in the presence of the GTPase ρ [38,39]. This is shown in Fig. 3(a).

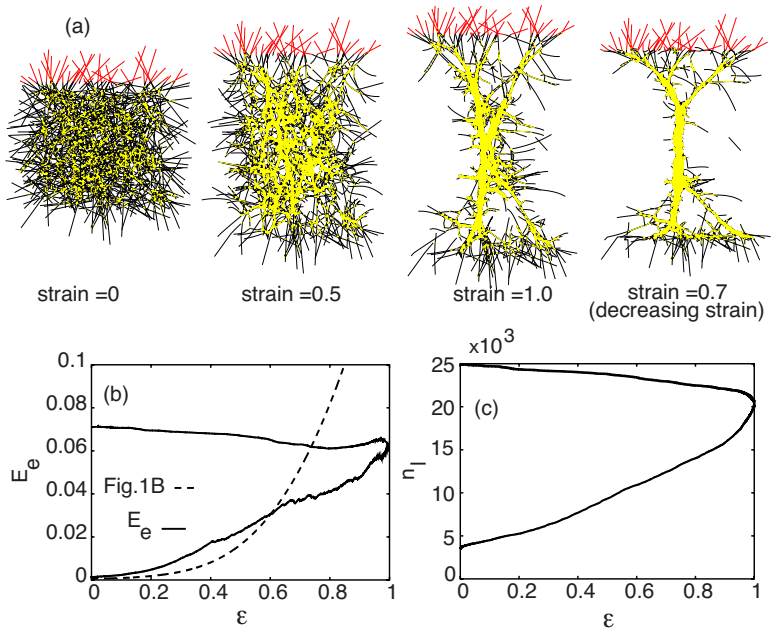

FIG. 3. (Color online) (a) Snapshots of a mesh with dynamic cross-links at $\epsilon = 0.0$, 0.5, 1.0, 0.7. The first three snapshots are prior to the stress maximum while the last is after maximum strain is reached. (b) Elastic energy (E_e) of the fibers for the mesh in (a) as a function of strain ϵ (full line). Dashed line: curve from Fig. 1(b) for comparison. (c) Number of cross-links as a function of ϵ. The curves on the top in (b) and (c) are obtained during destraining.

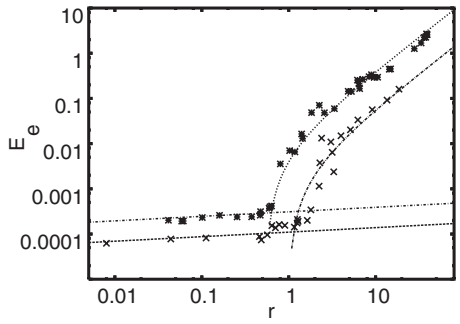

FIG. 4. Elastic energy (E_e) as a function of the average number of cross-links per fiber (r) for 250 (crosses) and 750 (stars) fibers. Below the transition, the elastic energy has a weak dependence on r and above the critical value $E_e \sim (r-r_c)^{1.5}$.

The mesh with dynamic cross-links has the highest initial stiffness of all three cases studied. The formation of stress on fibers is to a large extent irreversible and the stiffness increases in the same manner as for passive cross-links [Fig. 3(b)].

Figure 3(c) shows that the number of links increases from about 3500 at zero strain to about 20 000 at maximum strain. As can be further seen in Fig. 3(c), the number of links continues to increase during destraining and the fiber bundles do not decompose. That means that the tension in the fiber bundle does not vanish during destraining. This indicates that the equilibrium configuration for the mesh with dynamic cross-links is a maximally dense compact packing of the fibers. Once formed, the elastic energy in the bundle is not enough to break the links. Making the breaking thresholds of the cross-links dependent on fiber tension would alter this behavior. This issue will be addressed in a separate study.

IV. COMPARISON WITH EXPERIMENTS

To be more quantitative, we have compared our model simulations against the experimental results of Lieleg *et al.* [4]. In their experiment they had a solution of actin filaments and actin-binding protein called fascin. In other words, fascin is the cross-linker. Lieleg *et al.* showed that when the cross-linker concentration increases above a critical value, the actin filaments self-organize to form a homogeneous network, i.e., they saw a transition from an entangled solution to what they call "a cross-linked bundle phase"; the network was reported to consist of actin bundles as its structural unit, which is very similar to our observations as seen in Fig. 3(a).

We measured the elastic energy of the network, which corresponds to the measurement of the stiffness by Lieleg *et al.*, since those quantities scale similarly. The molar ratio of cross-linkers in the experiment corresponds to the average number of cross-links per fiber in our simulations.

Figure 4 shows the elastic energy at small strain as a function of the average number of cross-links per fiber for systems of 250 and 750 filaments (r corresponds to the molar ratio R of fascin in Ref. [4]). Above the transition, the elastic energy scales as $E_e \sim (r-r_c)^{1.5}$ which is the same scaling as found by Lieleg *et al.* (see Fig. 2 in Ref. [4]). The crossover can be seen as a percolation threshold.

In Fig. 5, we plot stress-strain curves for three different values of the average number of cross-links per fiber, $r = 1.78$, 2.86, and 5.05. Figure 5(a) shows that the initial slope is higher for larger r, corresponding to larger stiffness. As strain is increased, the cross-links start to break, which leads to reduced stiffness and to the sawtooth patterns seen in the figure. The cross-links start to break earlier, i.e., at a smaller strain, for a larger value of r. Figure 5(b) shows the strain at which the first cross-links break as r is varied. The line corresponds to r^{-1}, which is exactly the same scaling as observed by Lieleg *et al.*

V. CONCLUSIONS

To summarize, we have studied actin filament networks using three hierarchical models of increasing complexity: passive, semipassive, and a dynamic network which is able to adjust its cross-links dynamically. The networks show increasingly complicated behavior. We find strain hardening without entropic elasticity, avalanches of cross-link slippage leading to strong strain softening in the case of breakable cross-links, and spontaneous formation of stress-carrying fiber bundles in the case of dynamic cross-links. Support for our findings is given by the experiments of Rosenblatt *et al.* [40], who found that in human airway smooth muscle the ratio between dynamic and passive may control the nature of stiffening. To make a direct connection to experiments, we

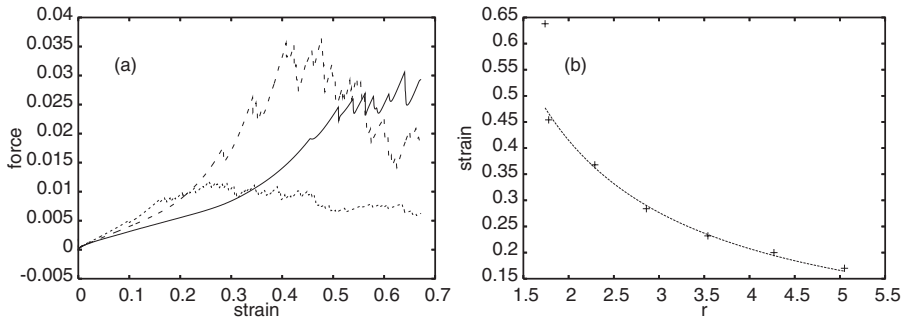

FIG. 5. (a) Stress-strain curves for three different values of average number of crosslinks per fiber, $r = 1.78$ (solid line), 2.86 (dashed), and 5.05 (dotted). The initial slope is higher for larger r, corresponding to larger stiffness. The sawtooth pattern results from breaking of cross-links, and such breakings reduce stiffness. As could be expected, cross-links break at smaller strain for larger r. (b) Strain at which the first cross-link breaks as a function of r. The scaling (the line) is the same as that found by Leileg *et al.*, i.e., r^{-1}.

compared our simulations to the results of Lieleg *et al.* [4] and found excellent agreement. They also report bundle formation, which is exactly what we see in our simulations with dynamic cross-linkers.

We would also like to mention the experiments by Chaudhuri *et al.* [41], which indicate that filament properties, cross-link density, and the dynamic nature of cross-links play a crucial role in controlling network stiffness, as both strain hardening and subsequent softening is observed in dendritic actin networks. They also point out the possibility of buckling as the mechanism behind softening. It is possible that cross-link density controls the selection between different softening mechanisms. We are currently addressing those issues in detail.

ACKNOWLEDGMENTS

P.B.S.K. thanks P. Pullarkat and P. Fernández for discussions. Financial support from the Academy of Finland (I.V., P.B.S.K.) and NSERC of Canada (M.K.) is acknowledged. Computational resources were provided by the Finnish IT Center for Science, the SharcNet grid computing facility (www.sharnet.ca), and the HorseShoe supercluster computing facility at the University of Southern Denmark.

[1] D. Bray, *Cell Movements*, 2nd ed. (Garland, New York, 2001).
[2] D. C. Morse, Phys. Rev. E **58**, R1237 (1998).
[3] R. Tharmann, M. M. A. E. Claessens, and A. R. Bausch, Phys. Rev. Lett. **98**, 088103 (2007).
[4] O. Lieleg, M. M. A. E. Claessens, C. Heussinger, E. Frey, and A. R. Bausch, Phys. Rev. Lett. **99**, 088102 (2007).
[5] M. L. Gardel, M. T. Valentine, J. C. Crocker, A. R. Bausch, and D. A. Weitz, Phys. Rev. Lett. **91**, 158302 (2003).
[6] K. Sekimoto, N. Mori, K. Tawada, and Y. Y. Toyoshima, Phys. Rev. Lett. **75**, 172 (1995).
[7] S. Halpain, Nat. Neurosci. **6**, 101 (2003).
[8] J. Howard, *Mechanics of Motor Proteins and the Cytoskeleton*, 1st ed. (Sinauer Associates, Sunderland, MA, 2001).
[9] J. van der Gucht, E. Paluch, J. Plastino, and C. Sykes, Proc. Natl. Acad. Sci. U.S.A. **102**, 7847 (2005).
[10] A. C. Maggs, Phys. Rev. E **57**, 2091 (1998).
[11] F. C. MacKintosh, J. Käs, and P. A. Janmey, Phys. Rev. Lett. **75**, 4425 (1995).
[12] E. Frey, K. Kroy, J. Wilhelm, and E. Sackmann, in *Dynamical Networks in Physics and Biology*, edited by G. Frogacs and D. Beysens (Springer-Verlag, Berlin, 1998), pp. 1–16.
[13] D. A. Head, A. J. Levine, and F. C. MacKintosh, Phys. Rev. Lett. **91**, 108102 (2003).
[14] D. Humphrey, D. Duggan, D. Saha, D. Smith, and J. Käs, Nature (London) **416**, 413 (2002).
[15] A. J. Levine, D. A. Head, and F. C. MacKintosh, J. Phys.: Condens. Matter **16**, S2079 (2004).
[16] M. L. Gardel, J. H. Shin, F. C. MacKintosh, P. Matsudaira, and D. A. Weitz, Science **304**, 1301 (2004).
[17] C. Storm, J. J. Pastore, F. C. MacKintosh, T. C. Lubensky, and P. A. Janmey, Nature (London) **435**, 191 (2005).
[18] M. F. Coughlin and D. Stamenovic, Biophys. J. **84**, 1328 (2003).
[19] C. Heussinger and E. Frey, Phys. Rev. Lett. **96**, 017802 (2006).
[20] O. Medalia, I. Weber, A. S. Frangakis, D. Nicastro, G. Derisch, and W. Baumeister, Science **298**, 1209 (2002).
[21] D. Boal, *Mechanics of the Cell*, 1st ed. (Cambridge University Press, Cambridge, U.K., 2002).
[22] P. Bursac, G. Lenormand, B. Fabry, M. Oliver, D. A. Weitz, V. Viasnoff, J. P. Butler, and J. J. Fredberg, Nat. Mater. **4**, 557 (2005).
[23] P. R. Onck, T. Koeman, T. van Dillen, and E. van der Giessen, Phys. Rev. Lett. **95**, 178102 (2005).
[24] D. Mizuno, C. Tardin, C. F. Schmidt, and F. C. Mackintosh, Science **315**, 370 (2007).
[25] K.-J. Bathe, *Finite Element Procedures in Engineering Analysis* (Prentice-Hall, Englewood Cliffs, NJ, 1982).
[26] L. D. Landau and E. M. Lifshitz, *Theory of Elasticity*, 3rd ed. (Pergamon, Oxford, 1986).
[27] S. R. Wu, Comput. Methods Appl. Mech. Eng. **195**, 44 (2006).
[28] C. Wei-zang, Appl. Math. Mech. **3**, 319 (1982).
[29] F. Ziebert and I. S. Aranson, Phys. Rev. E **77**, 011918 (2008).
[30] J. A. Åström, J. P. Mäkinen, M. J. Alava, and J. Timonen, Phys. Rev. E **61**, 5550 (2000).
[31] J. Wilhelm and E. Frey, Phys. Rev. Lett. **91**, 108103 (2003).
[32] N. Scafetta and B. J. West, Phys. Rev. Lett. **92**, 138501 (2004).
[33] M. E. J. Karttunen, K. J. Niskanen, and K. Kaski, Phys. Rev. B **49**, 9453 (1994).
[34] L. I. Salminen, A. I. Tolvanen, and M. J. Alava, Phys. Rev. Lett. **89**, 185503 (2002).
[35] A. Guarino, S. Ciliberto, A. Garcimartin, M. Zei, and R. Scorretti, Eur. Phys. J. B **26**, 141 (2002).
[36] J. Åström *et al.*, Phys. Lett. A **356**, 262 (2006).
[37] J. A. Åström, J. Timonen, M. Myllys, J. Fellman, and J. LeBell, Eur. Phys. J. E **22**, 61 (2007).
[38] M. Chrzanowska-Wodnicka and K. Burridge, J. Cell Biol. **133**, 1403 (1996).
[39] R. Kaunas, P. Nguyen, S. Usami, and S. Chien, Proc. Natl. Acad. Sci. U.S.A. **102**, 15895 (2005).
[40] N. Rosenblatt, S. Hu, B. Suki, N. Wang, and D. Stamenović, Ann. Biomed. Eng. **35**, 224 (2007).
[41] O. Chaudhuri, S. H. Parekh, and D. A. Fletcher, Nature (London) **445**, 295 (2007).